scientific reports

Check for updates

OPEN

A digital twin framework for forensic reconstruction of alcohol intake via fast and slow metabolite kinetics

Henrik Podéus[1], Christian Simonsson[1], Gerd Jakobsson[2,3], Robert Kronstrand[2,3], Elin Nyman[1], William Lövfors[1,6] & Gunnar Cedersund[1,4,5,6]✉

Accurately determining the timing and/or amount of consumed alcohol is critical in healthcare and forensic contexts, yet self-reported data are often unreliable due to stigma and legal implications. Objective biomarkers are therefore essential. Commonly used markers such as *blood*- and *breath alcohol concentrations* (BAC, BrAC) decline rapidly, limiting their utility for reconstructing drinking scenarios. Such reconstructions are essential for legal assessments, including refuting the "hipflask" defence. Markers with slower kinetics, such as *ethyl glucuronide* (EtG), *ethyl sulphate* (EtS), and *urine alcohol concentration* (UAC) provide complementary temporal information; however, current approaches fail to fully exploit available data. Here, we introduce a unified physiological digital twin that mechanistically integrates BAC, BrAC, EtG, EtS, and UAC within a single framework. This model captures the joint dynamics of rapid- and slower markers, enabling personalized simulations of alcohol intake and metabolism. We show that this integrated approach substantially improves reconstruction of past drinking events and supports complex forensic assessments requiring high temporal precision. To ease practical application, we provide an interactive web tool that allows users to evaluate hypothetical drinking scenarios and visualise individualized biomarker trajectories. Our work establishes a foundation for precision modelling of alcohol kinetics, bridging gaps between clinical, forensic, and computational domains.

Keywords BAC, EtG, UAC, mathematical modelling, judicial support, DUIA

Abbreviations

BAC	blood alcohol concentration
BMI	body mass index
BrAC	breath alcohol concentration
DUIA	driving under the influence of alcohol
EtG	ethyl glucuronide
EtS	ethyl sulphate
SEM	standard error of the mean
PEth	phosphatidylethanol
TBW	total body water
UAC	urine alcohol concentration

Alcohol consumption is associated with a range of societal, health, and legal challenges, including cases of *driving under the influence of alcohol* (DUIA). A problem in the forensic analysis of DUIA cases is the so called 'hipflask' defence, where a person claims to have ingested alcohol only post-accident. These claims are hard to

[1]Department of Biomedical Engineering (IMT), Linköping University, Linköping 58185, Sweden. [2]Department of Forensic Genetics and Forensic Toxicology, National Board of Forensic Medicine, Linköping, Sweden. [3]Department of Biomedical and Clinical Sciences, Division of Drug Research, Linköping University, Linköping, Sweden. [4]Center for Medical Image Science and Visualization (CMIV), Linköping University, Linköping, Sweden. [5]School of Medical Sciences and Inflammatory Response and Infection Susceptibility Centre (iRiSC), Faculty of Medicine and Health, Örebro University, Örebro, Sweden. [6]William Lövfors and Gunnar Cedersund contributed equally to this work. ✉email: gunnar.cedersund@liu.se

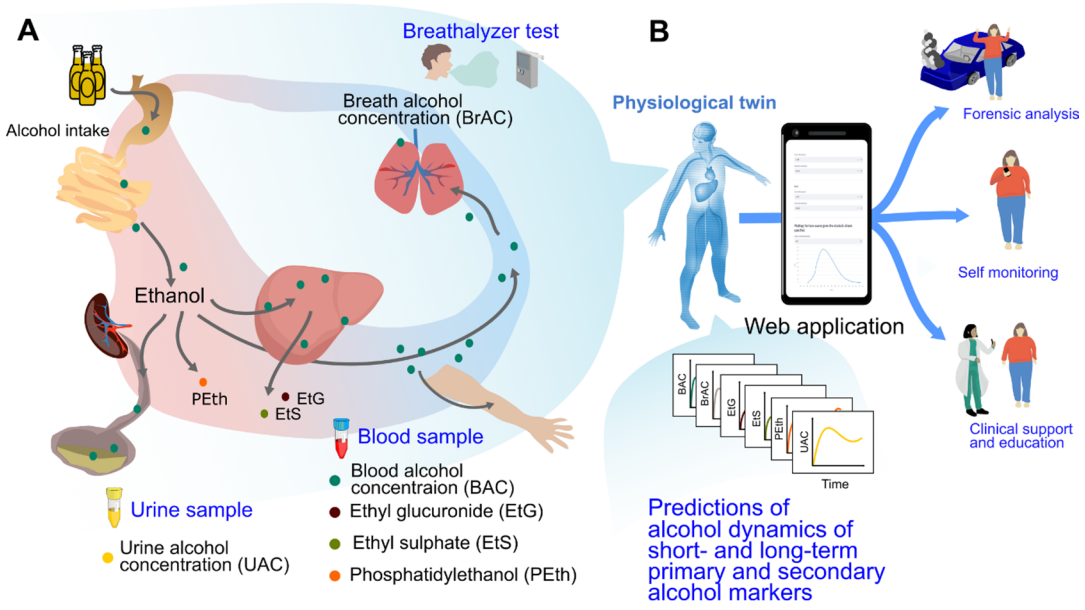

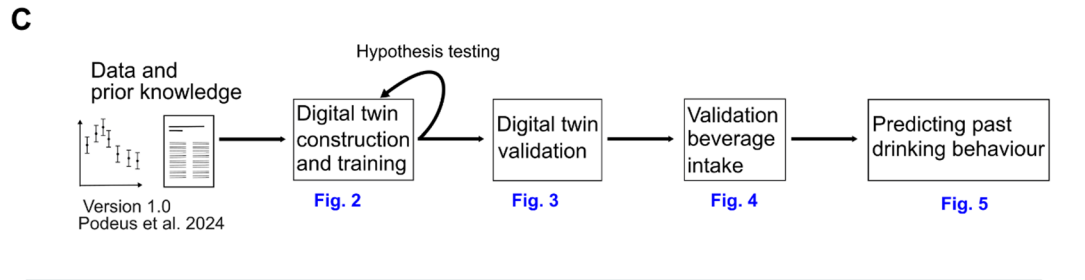

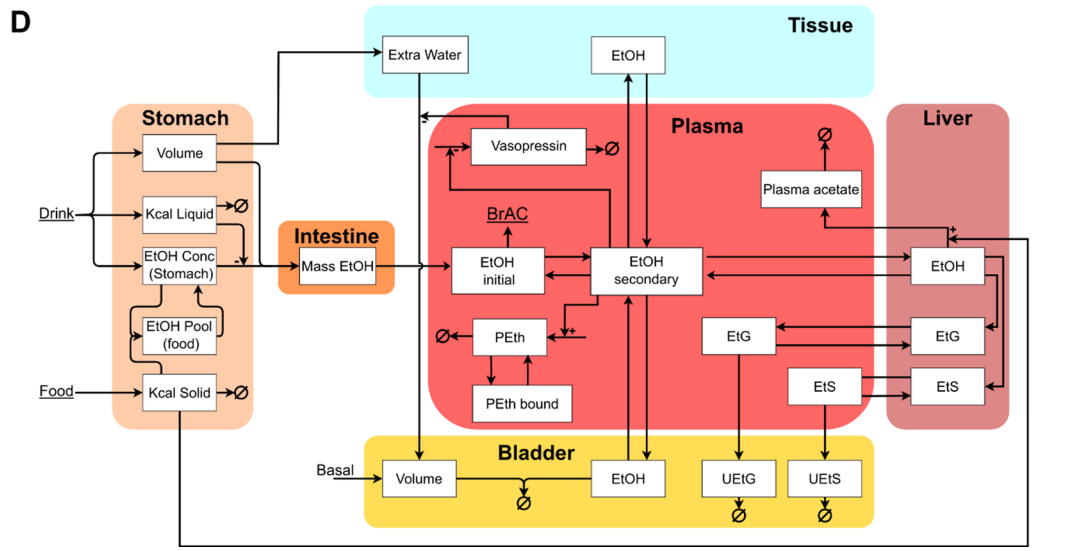

disprove in the forensic analysis due to the rapid absorption of alcohol and challenges in reconstructing and validating drinking scenarios.

The difficulty in validating drinking scenarios stems from the available tools and measured data. Traditionally short-term markers of alcohol consumption, such as *blood alcohol concentration* (BAC) and *breath alcohol concentration* (BrAC), have been used in forensic analysis of DUIA[1–3]. While reliable, the information available in these markers are limited by: the fast absorption- and elimination phase[4,5], dependence on anthropometrics[6,7], and paired consumption with other liquids and foods[8–10]. Consequently, short-term markers are incapable of accurately determining the timing of the alcohol intake – which is needed to verify/disprove the 'hipflask' defence[11–13]. To address this issue, new markers such as *ethyl glucuronide* (EtG), *ethyl sulphate* (EtS), and *urine alcohol concentration* (UAC) with a slower rate of appearance have been considered for the forensic analyses adding time-sensitive information[4,14]. Integrating these metabolite profiles could potentially enable

◀**Fig. 1**. Study overview. **A)** The physiological digital twin presented in this work describes the dynamics of various ethanol markers: breath alcohol concentration (BrAC), blood alcohol concentration (BAC), urine alcohol concentration (UAC), blood ethyl glucuronide (EtG), blood ethyl sulphate (EtS), and phosphatidylethanol (PEth). **B**) The digital twin can offer predictions of the time profiles of the various ethanol markers, which could be valuable in several possible use-cases. For availability the framework is provided in a web application. **(C)** In this work we develop a physiological digital twin that incorporates existing knowledge and data of different drinking scenarios from ten studies. After the model development and validation, the model can make predictions of unknown drinking behaviour from available data samples. **(D)** The model consists of: (i) a stomach compartment that handles the interactions of alcoholic beverages, non-alcoholic beverages, and food, (ii) an intestine compartment from where the alcohol is absorbed into, (iii) a plasma compartment from which ethanol contributes to PEth formation and distributed into either, (iv) the bladder where UAC is present, (v) the tissue, or (vi) the liver where EtG and EtS are synthesized. BrAC is expressed from the plasma ethanol levels in the central compartment.

reconstruction of prior drinking events. However, fully extracting the information contained in the intersection of these profiles requires advanced analytical approaches, such as mathematical modelling.

Mathematical modelling has historically been a fundamental tool for estimating the consumption of alcohol, using e.g., Widmark formula[15] or BAC focused models[16–19], typically relying on the elimination rate of alcohol. More recent models describe the appearance and kinetics of either EtG or EtS[20,21], following single intakes of alcohol. However, no current model can describe all the previously mentioned markers of alcohol consumption and are typically limited to very simple drinking patterns. Additionally, for mathematical models to be of use in forensic analysis they need to be highly individualizable – something typically achieved by digital twins[22–24]. We have previously presented such a digital twin model for alcohol consumption[25], that connects BAC and BrAC profiles with the long-term alcohol blood marker *phosphatidylethanol* (PEth). By extending the framework with the EtG, EtS, and UAC pathways, our tool could be used to extract the time-sensitive information needed for a more comprehensive and accurate forensic analysis of drinking scenarios.

Here, we extend our physiological digital twin to integrate BAC, EtG, EtS, and UAC into a unified mechanistic framework. This approach enables simultaneous modelling of short- and long-term alcohol markers, providing a comprehensive representation of drinking behaviour. We further demonstrate that the model can be personalized to new individuals and used to reconstruct drinking events across a range of scenarios, enabling more rigorous forensic evaluation—including in situations where current methodologies struggle, such as assessments of hipflask-defence claims.

Results

We have constructed a mechanistic model (Fig. 1D) describing the dynamics of alcohol metabolites with fast- and slow kinetics based on our previous work[25]. The new model features include: (i) addition of the metabolic interactions of EtG and EtS in the liver and the following uptake in the plasma[4,14], (ii) introduction of the bladder compartment and the elimination of BAC via the urine, i.e. UAC dynamics[4]. Urine-based elimination of EtG and EtS was also added. (iii) introduction of a tissue compartment and a formulation of *total body water* (TBW)[26], allowing more accurate distribution of BAC, (iv) splitting the plasma compartment into a central- and peripheral plasma compartment, to better describe the BrAC dynamics, (v) introduction of a diuretic effect through the arginine-vasopressin interactions[27,28], and (vi) added an upregulation of enzymatic alcohol elimination when food is present in the stomach[29–31].

The model was trained and validated on various published experimental data[9,29,32–38], including dual-drink data from Hoiseth et al.[11] and Kronstrand et al.[12]. The model captures all key behaviours in the estimation data (Figs. 2 and 3, S1-S3). The model was also validated against independent data, data from Wang et al.[38]. (Fig. 4). To highlight how the model could be used as a digital twin for all short-term markers, the model was used to predict the alcohol marker profiles (previously unpublished data) of two distinct individuals (Fig. 5B-I). Lastly, we showcase how the model can be used as a support in, i.e., forensic cases where time profiles of alcohol elimination are investigated – for instance in cases of hipflask defence (Fig. 5J-Y). Based on this forensic scenario we provide a framework of analysis in an interactive web application (see code availability).

The model can describe EtG, EtS and UAC dynamics

The new developed model was simultaneously trained on data from 10 studies[9,11,12,29,32–37]. As already shown in our previous study[25], there is a good agreement between the model and all included studies of single-drink intake[9,29,32–37], see Fig. S1-S3. To also include data on a sequential drink scenario, and EtG, EtS and UAC, we extended the model training with data presented by Kronstrand et al. [12] and Hoiseth et al. [11]. This new data presents the behaviour of BAC (Fig. 2A-J), UAC (Fig. 2K-T), EtG (Fig. 3A-G), and EtS (Fig. 3H-N) in response to two sequential drinks ('x', single data points and means with error bars). All different drinking configurations in these two studies, included a first drink of beer with the alcohol content of 0.51 g/kg body weight, followed by a second drink of either: whiskey (Fig. 2A, E, I, K, O and S), vodka (Figs. 2B, F, J, L, P and T and 3A, D, G, H, K and N), beer (Figs. 2C, G, M and Q and 3B, E, I and L), or wine (Figs. 2D, H, N and R and 3C, F, J and M). The colour represents the dose of the second drink (blue - low dose of 0.25 g/kg, purple - medium dose of 0.51 g/kg, and red - high dose of 0.85 g/kg). The best model simulation is presented with solid lines and the model uncertainty as a shaded area. There was a good simultaneous agreement with all training data, confirmed by a visual assessment and a χ^2 test. The χ^2 test statistic was 642.7 which was lower than the cutoff ($T_{\chi 2}$=735.5, for n=674).

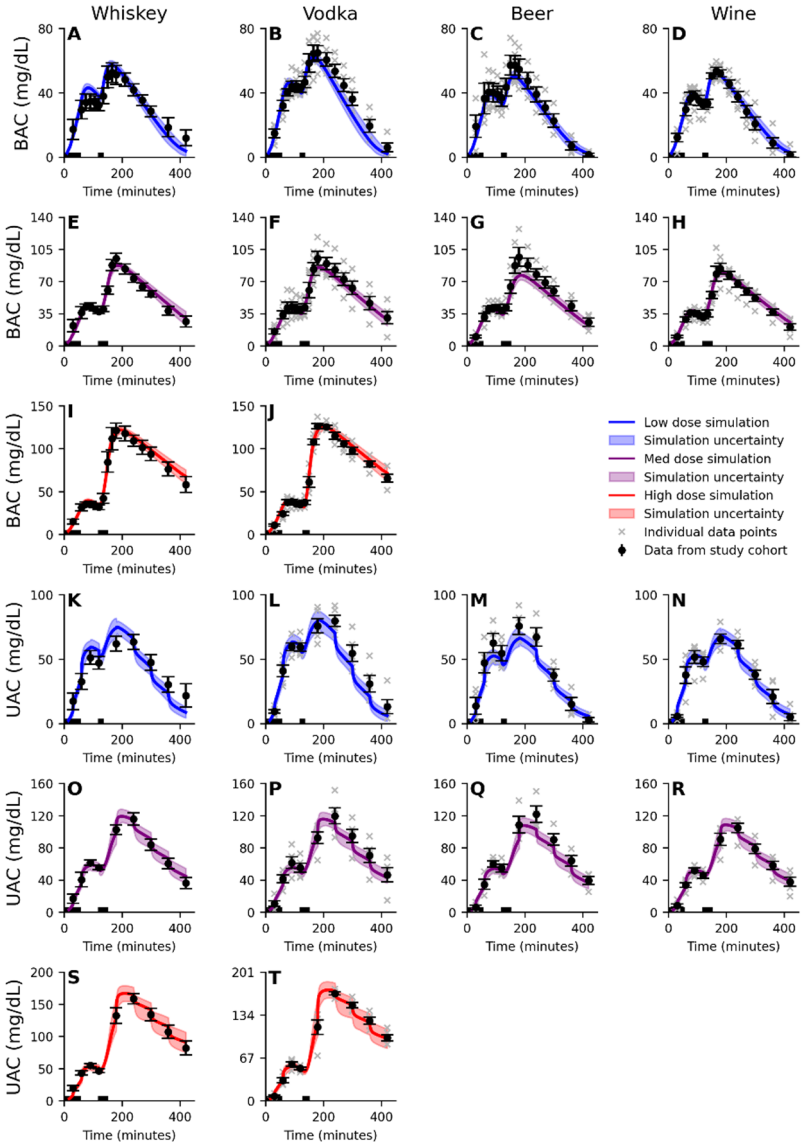

Fig. 2. Model agreement to the BAC and UAC data. The solid line is the best model fit (simultaneous agreement to all estimation data), the shaded area is the model uncertainty, the error bars is the standard error of the mean (SEM), and the 'x' notations indicate the reported individual data points. The model (shaded area) describes the dynamics of the **A-J)** blood alcohol concentration (BAC), **K-T)** urine alcohol concentration (UAC). All experiments includes a first drink of beer with a 0.51 g/kg dose of ethanol, consumed in 4 periods of 10 min over 60 min, and a second drink of varying doses, 0.25 g/kg (blue), 0.51 g/kg (purple), or 0.85 g/kg (red), composed of either; whiskey (A, E, I, K, O, S), vodka (B, F, J, L, P, T), beer (C, G, M, Q), or wine (D, H, N, E). The second drink was consumed over 15 min (low dose) or 30 min (medium and high dose). The periods where the drinks are consumed are indicated by the black bar over the x-axis. Meals were consumed after the start (300 kcal) of the session and 180 min into (500 kcal) the study.

Model validation of alcohol markers

Following the model training, the model was validated against an independent data set from Wang et al.[38], see Fig. 4A, E and G. The subjects in the study consumed 0.119 L of vodka (40 v/v%), together with a meal of 500 kcal, over 30 min and BAC, EtG, and EtS were measured in blood at several time points over 720 min. This independent study was first simulated with the model and then compared with the data from Wang et al.[38]. The model validation also passed the χ^2 test and the model uncertainty is shown as the shaded area (Fig. 4A, C, E and G). The χ^2 test statistic was 28.04 which was lower than the cutoff (T_{χ^2}=31.41, for n=20). The model was further evaluated by performing a sensitivity analysis where the anthropometrics were varied to represent the variability of a population (age 20–80 years, *body mass index* (BMI) 18–32 kg/m^2, and a height of 1.5–1.8 m for females and 1.6–1.95 m for males). The model simulations of this population, given the same drinking scheme presented by Wang et al.[38], are presented as the blue-green gradient (Fig. 4B, D, F and H), where the gradient indicate the TBW in litre (L) of the subjects, which is influenced by all the anthropometric variables (see Eq. 9). These

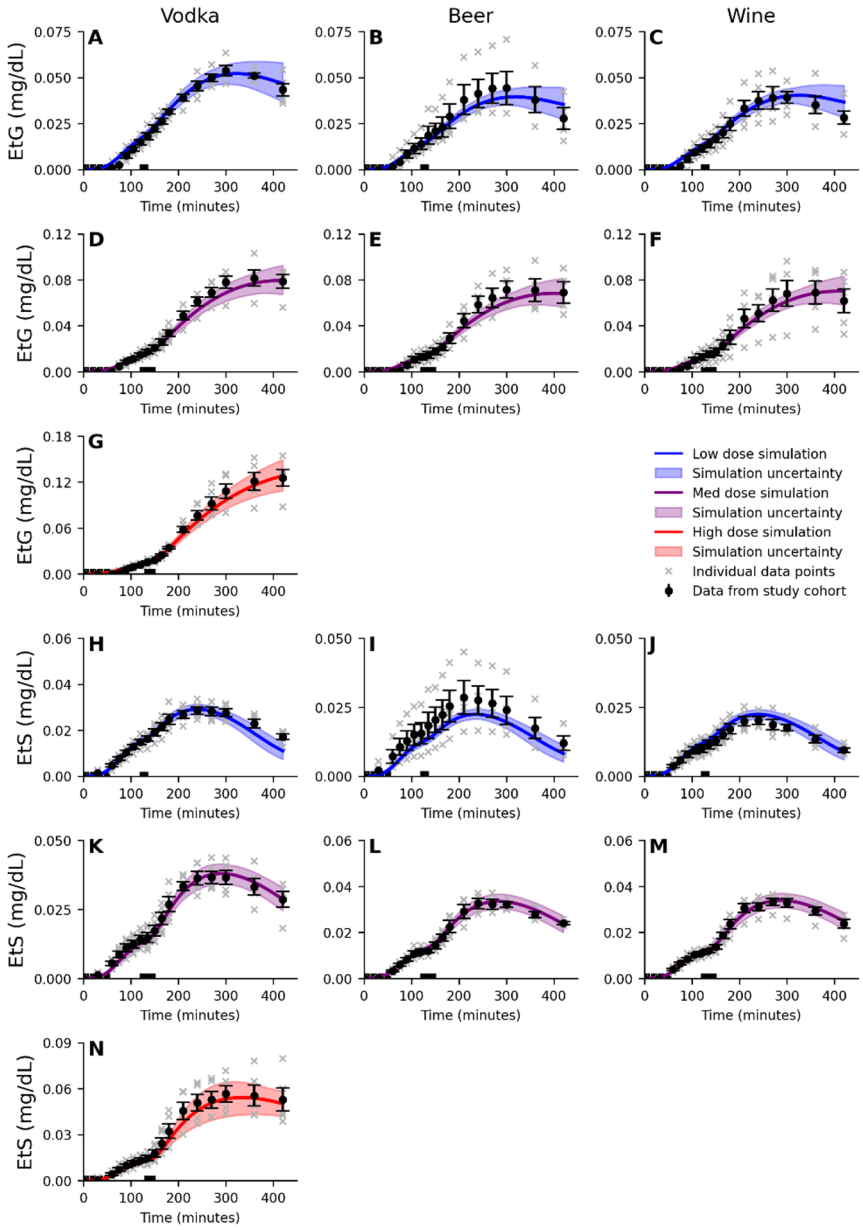

Fig. 3. Model agreement to the EtG and EtS data. The solid line is the best model fit (simultaneous agreement to all estimation data), the shaded area is the model uncertainty, the error bars is the standard error of the mean (SEM), and the 'x' notations indicate the reported individual data points. The model (shaded area) describes the dynamics of the **A-G)** blood ethyl glucuronide concentration (EtG), **H-N)** blood ethyl sulphate concentration (EtS). All experiments includes a first drink of beer with a 0.51 g/kg dose of ethanol, consumed in 4 periods of 10 min over 60 min, and a second drink of varying doses, 0.25 g/kg (blue), 0.51 g/kg (purple), or 0.85 g/kg (red), composed of either; vodka (A, D, G, H, K, N), beer (B, E, I, L), or wine (C, F, J, M). The second drink was consumed over 15 min (low dose) or 30 min (medium and high dose). The periods where the drinks are consumed are indicated by the black bar over the x-axis. Meals were consumed after the start (300 kcal) of the session and 180 min into (500 kcal) the study.

simulations highlight the robustness of the model, as the model behaviour is qualitatively preserved between the individuals over the whole population, which is of importance in applications of model personalization. We next investigated how well the validated model functions in additional use cases, including personalized predictions for single individuals.

Model prediction of individual alcohol marker profiles

Following the validation and sensitivity analysis, the model's ability to make personalized prediction was evaluated using newly collected data from single individuals (Fig. 5A). The data includes BAC, UAC, EtG, and EtS for sequential drinks and the raw data is available in the Supplementary Information, see "S1 Raw prediction

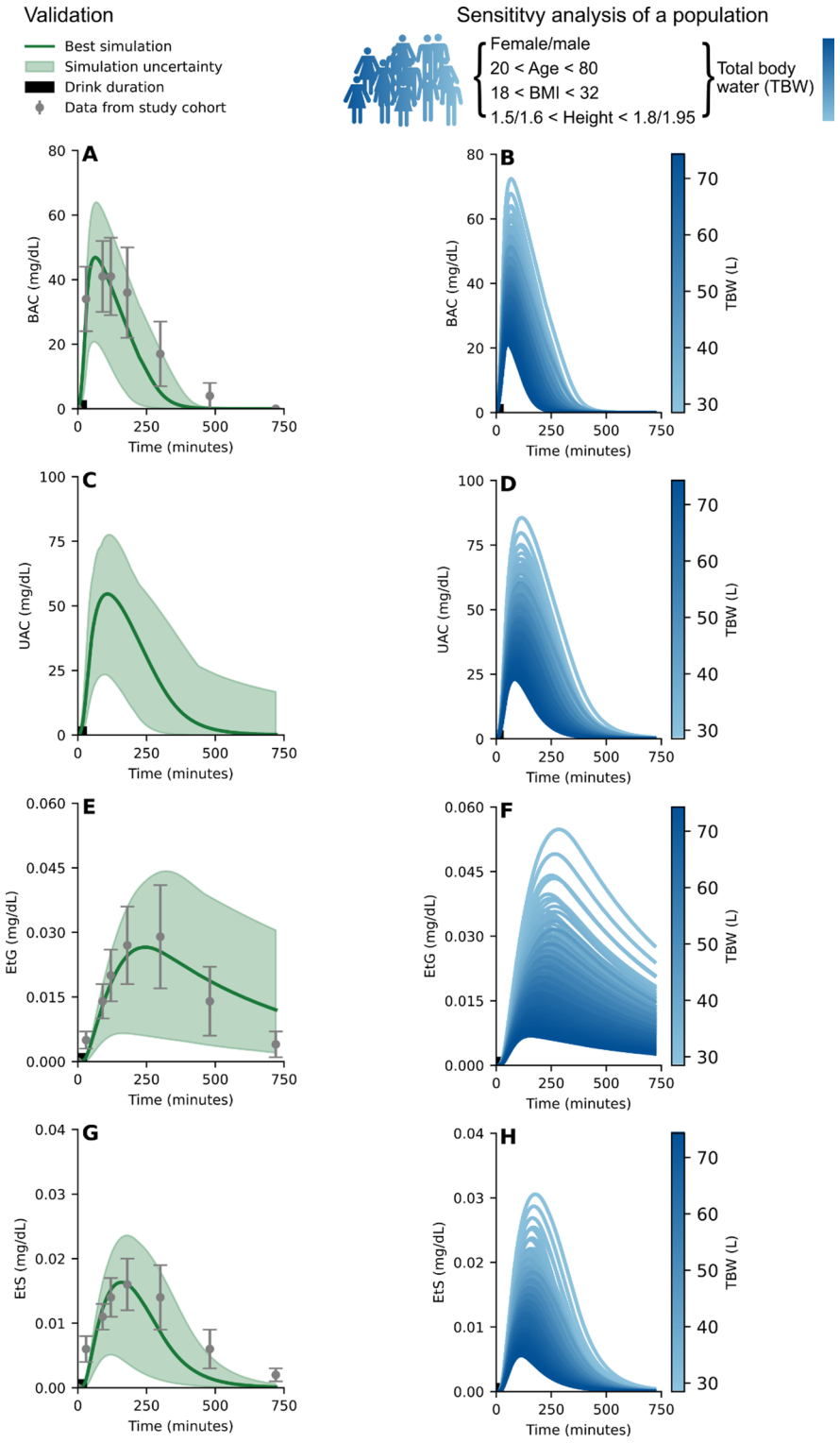

data". The study was approved by the Swedish Ethical Review Authority, 2023-02640-01, see methods. The data describes two individuals, a male (Fig. 5B-E, orange), body weight 106.6 kg, age 28 years, height 1.86 m, TBW 66.2 L, blood volume 6.4 L, and female (Fig. 5F-I, pink), bodyweight 62.7 kg, age 22 years, height 1.69 m, TBW 37.4 L, blood volume 4.0 L. The model prediction, shaded area, aligns well with the experimental data, black circles, (Fig. 5B-I) indicating that although the model is trained on a mean population behaviour it can be used for predictions of individuals. The drinking-challenge for the male and female were consumption of an initial drink containing 0.85 g/kg ethanol composed of 13 v/v% wine over four 10 min block for a total of 60 min and a second drink containing 0.51 g/kg ethanol composed of 20 v/v% vodka consumed over 30 min. Meals (300 kcal, 500 kcal, and 500 kcal) were consumed at 90-, 180-, and 540 min for the male, and 30-, 180-, and 540 min for the female.

◀**Fig. 4**. Model validation and sensitivity analysis. The solid line is the simulation using the optimal parameters found for the best model fit to estimation data, the shaded area is the model uncertainty, the grey errorbars indicating the standard error of the mean (SEM) for the validation data. The model (shaded area) describes the dynamics of the: **(A)** blood alcohol concentration (BAC), **C**) urine alcohol concentration (UAC), **E)** blood ethyl glucuronide (EtG) concentration, and **G)** blood ethyl sulphate (EtS) concentration, given a beverage composed of 0.119 L of 40 v/v% spirits containing 0 kcal, consumed over 30 min (indicated by the black bar on the x-axis and paired with a meal of 500 kcal, consumed over the same 30 min duration. A sensitivity analysis was performed on a population with the anthropometrics ranging between; age 20–80 years, body mass index (BMI) 18–32 kg/m^2, heights of 1.5–1.8 m for females and 1.6–1.95 m for males. This population was challenged with the same drink and food pairing as in **A**, **C**, **E**, and **G** and the model simulations of the population are presented as the blue gradient for **(B)** BAC, **D)** UAC, **F)** EtG, and **H)** EtS. The blue gradient corresponds to the volume of total body water (TBW) for the subjects.

As a showcase of the model's ability to accurately predict distinct drinking-challenges, and as such also separate between similar challenges, we present an alternative scenario. This in-silico scenario (Fig. 5J-Q) replaces both drinks with a single vodka challenge (1.0 g/kg ethanol) for the male (Fig. 5J-M) and female (Fig. 5N-Q). This scenario represents a plausible alternative drinking-challenge. For the in-silico scenario, the BAC profile closely aligns with segments of the experimental data (Fig. 5J and N) and would be hard to differentiate from the actual drinking-challenge (Fig. 5B and F). This highlights a current limitation in, for instance, forensic analysis of alcohol elimination. By making use of the model's ability to simultaneously describe all markers, we can distinguish between wide range of plausible drinking-challenges and offer insights of deviating elimination profiles, indicated by the green lines (Fig. 5J-Q). This example highlights how our physiological digital twin could be used as a decision support in forensic analysis.

Discussion

Herein, we present a physiological twin that can describe the dynamics of different markers of alcohol consumption: BAC (Fig. 2, S2), UAC (Fig. 2), EtG (Fig. 3), and EtS (Fig. 3), and PEth (Fig. S3). The model was validated using independent data (Fig. 4A, E, G), and the robustness was evaluated using a sensitivity analysis (Fig. 4B, D, F, H). The validated model was able to make personalized predictions of new individual data generated from dual drinking-challenge (Fig. 5B-I). Furthermore, we show how the model predictions can differentiate between similar drinking behaviours by simulating an in-silico drinking-challenge (Fig. 5J-Q). By evaluating the model predictions, the model can be used to differentiate between different claims of alcohol consumption. This capability could be utilized as a decision support tool in forensic analysis, where one needs to determine the time profile of alcohol elimination.

Model estimation, validation, and robustness analysis

The model was trained and validated to a total of ten different study datasets, which include different markers of ethanol consumption, including: BAC, UAC, EtG, EtS, and PEth (Figs. 2 and 3, S1-S3). An overview of the data is given in the Supplementary Information, "4 Usage of experimental data". The model could explain all estimation data (Figs. 2 and 3, S1-S3) and validation data (Fig. 4) to a satisfactory level. Altogether, the model sufficiently describes the dynamics of these ethanol consumption markers following consumption of beverages (single and dual) of different volumes, concentrations, time of consumption, in combination with food, and for individuals with different anthropometric data.

While the model passed a $\chi 2$-test for all estimation data, it is worth pointing out some aspects of the data that the model did not fully capture. Firstly, the model had some difficulty to describe the peak BAC following the consumption of the second drink of the medium dose of vodka (Fig. 2F) and beer (Fig. 2G), data presented by Hoiseth et al.[11]. In contrast, the model describes the medium dose well for whiskey (Fig. 2E), data presented by Kronstrand et al.[12], and wine (Fig. 2H), even though the dose of ethanol is the same as for beer and vodka. This difference points towards an inconsistency in the model explanation of the rate of gastric emptying. This discrepancy could stem from how the drink was consumed during the study, and what the drink was paired with, an aspect that we have explored in our previous work[25]. In the Hoiseth et al. study[11] and the Kronstrand et al. study[12], the consumption of non-alcoholic beverages was not recorded, and as such no alcohol-free drinks were included in the model inputs. Alcohol-free drinks were freely available during the experiment and were therefore likely consumed and could thus be the reason for the difference we observe in the medium dose. Secondly, we observe the same differences in peak UAC between vodka (Fig. 2P) and beer (Fig. 2Q), a too low peak, versus whiskey (Fig. 2O) and wine (Fig. 2R), a well described peak. This is expected as urine concentration is highly correlated with the blood concentration. Finally, one can note that the EtS concentration in the case of the low dose of beer (Fig. 3I) are underestimated. In this case, the experimental data is higher compared to the medium dose of beer (Fig. 3L) which is not mirrored in the BAC experimental data (Fig. 2C, G). The model does not have the ability to explain this difference in EtS synthesis, given similar BAC concentrations, and will therefore underestimate EtS for a low dose of beer. This behaviour could possibly be caused by a single subject with higher EtS synthesis (see grey 'x' markers, in Fig. 3I) which influences the mean behaviour not seen in the other groups.

There are also some qualitative differences between model predictions and corresponding validation data. For the validation, the model predicts a faster elimination of BAC than seen in the experimental data (Fig. 4A). As the model describes the rate of appearance of BAC well, one is inclined to believe that the drink is estimated well. Although the drinking-challenge is probably not fully representative to the one consumed in the Wang et

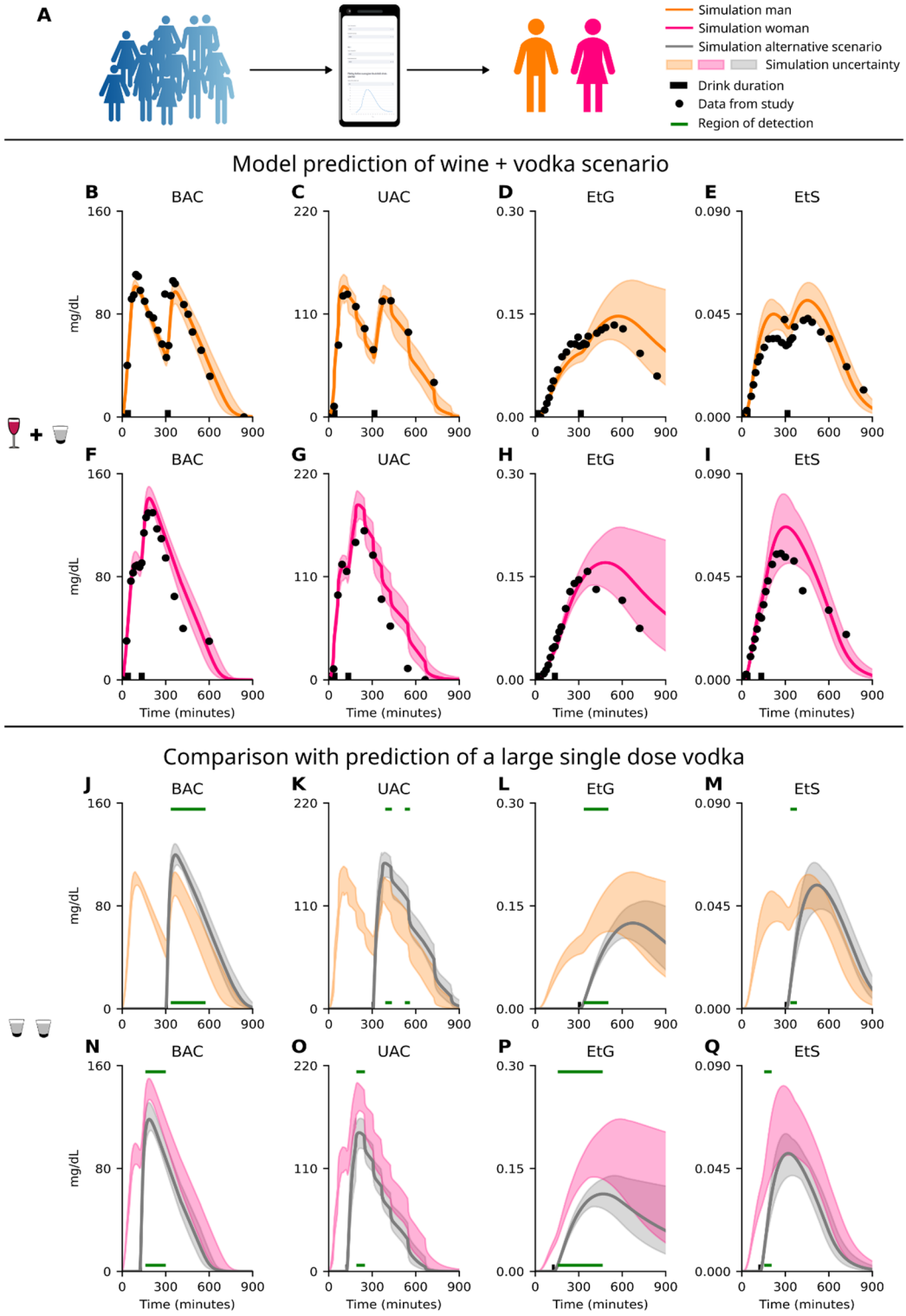

al. study[38], as the subject were tasked to consume a 40 v/v% beverage within 30 min and did likely not consume it evenly over this 30 min period (which we assume due to no other information available). Secondly, because of the rapid elimination of BAC we also observe a too fast clearance of EtS (Fig. 4G). Thirdly, we observe that the EtG instead is eliminated too slowly (Fig. 4E). This is likely a result due to the lack of EtG data showing the full elimination time-period in our model estimation data set. Since the model is not trained on the full elimination profile of EtG – the model predicts a slow elimination profile in the later, unknown, elimination phase. Finally, we can see that the model behaviour is preserved when challenging individuals within a population (age 20–80 years, *body mass index* (BMI) 18–32 kg/m^2, and a height of 1.5–1.8 m for females and 1.6–1.95 m for males) with the same drinking-challenge (0.119 L 40 v/v% over 30 min) (Fig. 4B, D, F, H). As expected, the drink has a higher influence on smaller individual (less TBW, light blue) and a lower influence on larger individuals (more TBW, dark blue).

◀**Fig. 5**. Model predictions of individuals in forensic scenarios. **A)** Illustration showing that the model is trained on a mean population behaviour and is now used to predict individual behaviours, a male (orange) and a female (pink). **B-I)** Model prediction of the four markers; **B** and **F)** blood alcohol concentration (BAC), **C** and **G)** urine alcohol concentration (UAC), **D** and **H)** blood ethyl glucuronide (EtG) concentration, and **E** and **I)** blood ethyl sulphate (EtS) concentration. The drinking-challenge for the male and female were consumption of an initial drink containing 0.85 g/kg ethanol composed of 13 v/v% wine over four 10 min block for a total of 60 min and a second drink containing 0.51 g/kg ethanol composed of 20 v/v% vodka consumed over 30 min. The solid line represents the best model solution from the model training, and the area is the model uncertainty. The data points are represented by the black circles, and the black bar indicates the period of alcohol consumption. **J-Q)** An in-silico drinking scenario for; **J-M)** the male and **N-Q)** the female, were evaluated. The alternative drinking-challenge was a single dose of 1.0 g/kg ethanol composed of 40 v/v% vodka for both the male and female. The model prediction is shown for the four different markers: **J** and **N)** BAC, **K** and **O)** UAC, **L** and **P)** EtG, and **M** and **Q)** EtS. The grey solid line represents the best model solution from the model training, and the grey area is the model uncertainty. The model prediction for the wine and vodka drinking-challenge (**B-I**) for the male is shown as reference for the male (orange **J-M**) and the female (pink, **N-Q**). The horizontal green lines indicate the regions where the model predicts differences between the two drinking-challenges for the respective individual (male and female).

Data considerations

Due to the lack of information in the different included studies some assumptions have been made and should be discussed. Firstly, some of the studies did not report anthropometrical data of the subjects or details regarding several aspects of the experimental setup e.g., reported drinking time. Also, for some datasets mean values were calculated in a mixed cohort including both female and male participants[11,12,35,36]. To take this into consideration we opted to estimate the mean blood volume based on the sex distribution. Also, for some studies the caloric content was not reported, leading to some assumptions regarding the consumed beverage. The caloric content is of importance as the gastric emptying module is the major contributor to the ethanol rate of appearance in plasma. For details regarding these assumptions see Supplementary Information "3 Input estimation". Secondly, the EtG and EtS concentrations were reported as zero until they exceeded the detection limit in the Hoiseth et al. study[11]. Since the subjects in the different groups pass the detection limit at different time points, we choose to exclude the data from the time points where all subjects had not reached the detection limit. In practice, EtS was part of the estimation data when time > 30 min and EtG was part of the estimation data when time > 75 min. Thirdly, as non-alcoholic beverages were available during the experiments in the Hoiseth et al. and Kronstrand et al. studies[11,12], we assumed that the participants consumed an equal volume of non-alcoholic beverages as the volume of 40 v/v% spirits (due to the large volume of hard spirits). This effectively doubles the volume and halves the concentration of the drink. Fourth, the study protocol in the Hoiseth et al. and Kronstrand et al. studies[11,12] included a blood sample every 15 min and a urine sample every 30 min during the drinking-challenge. We consider the effects of this as the first drink being consumed in four periods of ten minutes, leaving five minutes for data collection. Lastly, we decreased the drinking window for the high vodka challenge in Hoiseth et al.[11]. This is due to the BAC experimental data lagging and barely increasing 15 min into the reported drinking window. Compared to the high whiskey challenge in Kronstrand et al.[12], where BAC increases substantially faster, we assume that this discrepancy is due to hesitation of drinking. As such, we implement the vodka drinking-challenge to start ten minutes later, reduced the drinking window to twenty minutes.

The predictive capability of drinking behaviour of the model

The validated physiological twin was able to predict the profiles of the different alcohol markers, BAC (Fig. 5B and F), UAC (Fig. 5C and G), EtG (Fig. 5D and H), and EtS (Fig. 5E and I), for two new individuals – a large male (Fig. 5B-E) and a small female (Fig. 5F-I). While the predictions are generally impressive and points towards the robustness of the model, especially considering that only the anthropometric parameters in the model were tuned for these predictions, it is worthwhile to mention some deviations. While the BAC and UAC predictions are closely in line with the data (black circles, Fig. 5), EtG and EtS are a bit more deviating. This is not too surprising since the model was not able to fully describe the variability in the EtG and EtS levels during model training. This indicates that the model does not incorporate all the information needed to describe the inter-variability of EtG and EtS between individuals[39–41], resulting in the offset of the simulation and generally a larger uncertainty (shaded area). By investigating the variability in enzymatic expression of UDP-glucuronosylt ransferase[40,42] and sulfotransferase[43], one could better identify the individual differences and reduce the model variability. While this would be useful information and improve the physiological detail of the model, it is not feasible to always accompany the blood sample with an enzymatic test. Instead, the tuning would need to rely on further model development through larger data sets.

Altogether, our model advances the current state of mathematical models of alcohol kinetics[16–19], by integrating fast- and slow markers - BAC, EtG, EtS, UAC - into a single, unified framework. Previous studies have explored some marker relationships, such as EtG/BAC[20] or EtS/BAC[21]. For instance, Droenner et al.[20] proposed a model describing EtG dynamics and highlighted its potential for forensic applications, such as evaluating post-accident alcohol intake claims. However, these models are limited in scope: they do not capture overlapping metabolite dynamics and are generally restricted to simple, single-drink scenarios. Our approach addresses these limitations by enabling simultaneous modelling of fast- and slow metabolites across complex drinking patterns. Moreover, the framework introduces a mechanism for personalization through digital twins, allowing individual-specific parameterization. While still missing some personalization aspects, such as genetics[44,45] and

enzymatic expression[46,47], this capability not only enhances forensic accuracy but also opens the door to broader applications where individualized drinking behaviour reconstruction is critical.

The potential of physiological twins as support in forensic cases

The model was evaluated with an in-silico scenario (Fig. 5J-Q), constructed to be similar to the real drinking-challenge (Fig. 5B-I). This scenario consisted of a single larger drink of vodka (Fig. 5J-Q) and produced a model behaviour that described segments of the experimental data. But importantly, there are deviating behaviour between this scenario and the model prediction of the 'real' drinking-challenge (Fig. 5B-I). The regions that showcase the deviating behaviour is indicated by the green line (Fig. 5J-Q) and highlight where the model predictions of the original drinking-challenge (orange for male and pink for female) and the in-silico scenario (grey for both male and female) deviates from each other. Only regions after the consumption of the last drink had ended are highlighted. As can be seen, the different markers (BAC, UAC, EtG, and EtS) have different time intervals where the predicted behaviour deviates between the model predictions. This is of importance as it allows us to intersect the time profiles of the different markers to evaluate if the given scenario could have generated the experimental data. The different profiles of the markers also allow for a more robust evaluation of the claimed drinking-challenge, allowing the twin to identify small differences in the scenarios.

This capability could be of use in i.e. forensic analysis of DUIA cases, where one needs to determine if the claimed drinking-challenge is in accordance with the gathered data samples. Our model framework is well suited to offer support in such scenarios and to aid in the determination of the plausibility of a claimed scenario. To fully utilize the model framework, one would first need to investigate the sensitivity of the analysis depending on the delay between data sampling and the end of drinking and how the reliability of the different alcohol markers is affected with different number of data samples. Overall, the personalization capabilities of our modelling framework could improve the accuracy of the forensic analysis and aid in distinguishing between similar drinking-challenges.

In practical forensic settings, input information such as exact drinking times, drink sizes, or physiological characteristics may be incomplete or disputed. Within the proposed framework, such uncertainty does not prevent model use but will instead increase the uncertainty of the resulting predictions. Missing inputs can be explored through plausible ranges or estimated values, allowing the model to test whether a claimed drinking scenario could reasonably reproduce the observed biomarker profiles. Importantly, the primary purpose of the framework is to evaluate the plausibility of claimed scenarios rather than to provide a single deterministic reconstruction of events. When input information is incomplete, the resulting predictions therefore span a wider range of possible outcomes, which reduces the risk of overconfident conclusions. In this sense, uncertainty in the inputs translates into increased uncertainty in the model predictions, providing a conservative interpretation that is appropriate in forensic decision-support contexts.

Conclusion

To summarize, we present a unified physiological digital twin that accurately describe the dynamics of the alcohol markers: BAC, UAC, EtG, and EtS. This detail allows the physiological twin to reconstruct a broad spectrum of drinking scenarios. The twin generalizes well across individuals and differentiates between closely related consumption patterns, enabling more precise temporal assessments. Beyond its forensic relevance—including potential support in challenging DUIA evaluations such as the hipflask defence—the framework lays the groundwork for digital health applications in personalized risk assessment, behavioural monitoring, and clinical decision support.

Methods

Within this section the model equations are detailed, see Eqs. 2–9. The full model structure is shown in Fig. 1D.

Before detailing the equations, an example of an *ordinary differential equation* (ODE) is described. A typical ODE used in this work looks similar to Eq. (1).

$$\begin{aligned} \frac{d}{dt}(x) &= -va + vb \\ va &= ka \cdot x \\ vb &= kb \cdot input \end{aligned} \tag{1}$$

Here, *x* is a state in the model, *va* and *vb* are reaction rates, *ka* and *kb* are rate-determining parameters, and *input* is some input to the state. In other words, the amount of the state *x* is decreased by the reaction *va* with the speed *ka* and increased by the reaction *vb* with the speed *kb* depending on some input *input*.

Model description

This model was built upon our previous work, see Podéus et al.[25]. In the following sections, the changes and additions to the model are reported. The full model structure is available in the supplementary code, and the iterative model development is described in detail in the Supplementary Information, see "5 Changelog of rejected model structures".

Gastric emptying

The gastric emptying module was updated to the following format.

$$
\begin{aligned}
&\frac{d}{dt}\left(Vol_{stomach}\right) = +volDrinkPerTime - rvol_{emptying}\\
&\frac{d}{dt}\left(Kcal_{Liquid}\right) = +volDrinkPerTime \bullet kcalLiquidPerVol\\
&\frac{d}{dt}\left(Kcal_{remain}\right) = +volDrinkPerTime \bullet kcalLiquidPerVol\\
&-rvol_{emptying} \bullet \frac{Kcal_{remain}}{Vol_{stomach}}\\
&rvol_{emptying} = Vmax \bullet \left(\frac{Vol_{Change}}{Vol_{Change} + km}\right) \bullet kcal_{effect}\\
&Vol_{Change} = Vol_{stomch} - Vol_{stomach}\left(0\right)\\
&kcal_{effect} = \left(1 - \frac{\left(\frac{Kcal_{Liquid}}{k_{kcalscaling}}\right)^{n_{kcal}}}{\left(\frac{Kcal_{Liquid}}{k_{kcalscaling}}\right)^{n_{kcal}} + Km_{gastric}^{n_{kcal}}}\right)\\
&if new drink \rightarrow Kcal_{Liquid} = Kcal_{remain}
\end{aligned}
\tag{2}
$$

Here, the gastric volume is governed by the consumption of new liquids, *volDrinkPerTime*, and passing of liquid to the intestines, $rvol_{emptying}$. The caloric contents of the stomach are governed by the new $Kcal_{remain}$ state that: (i) keeps track of the incoming kcal, *kcalLiquidPerVol*, (ii) the emptying rate of kcal, and (iii) updates the $Kcal_{Liquid}$ state once a new drink is consumed.

Blood compartment split into central and peripheral

To account for the difference in rate of appearance in BrAC and BAC, the blood compartment was split into a central compartment, where BrAC is measured, and a peripheral compartment, where BAC is measured. The ethanol is absorbed into the central compartment, from the intestines, via $rEtOH_{uptake}$ as a mass (mg) and diluted into the blood volume of the central compartment. The ethanol then diffuses between the central and peripheral compartments, via $r_{Circulation}$. The downstream reactions, diffusion into the tissue $r_{Tissue\ Peripheral}$, uptake to the liver r_{Liver}, and transportation to, r_{Urine}, and from, $r_{Urine\ return}$, the bladder are feed from the peripheral compartment.

$$
\begin{aligned}
&\frac{d}{dt}BloodConc_{Central} = +\frac{rEtOH_{uptake}}{V_{BloodCentral}} - r_{Ciruclation}\\
&\frac{d}{dt}BloodConc_{Peripheral} = +r_{Circulation} \bullet \left(\frac{V_{BloodCentral}}{V_{BloodPeripheral}}\right)\\
&-r_{TissuePeripheral} - r_{Liver} + \left(-r_{Urine} + r_{Urinereturn}\right) \bullet V_{BloodPeripheral}\\
&rEtOH_{uptake} = MassEtOH_{Intestines} \bullet k_{EtOHuptake}\\
&r_{Circulation} = k_{equalize} \bullet \left(BloodConc_{Central} - BloodConc_{Peripheral}\right)\\
&r_{Liver} = k_{equlaizeLiver} \bullet \left(BloodConc_{Peripheral} - LiverConc\right)\\
&r_{Urine} = r_{Tissueurine} \bullet \frac{\left(BloodConc_{Peripheral}.V_{BloodPeripheral}\right)}{V_{PlasmaPeripheral}}\\
&+0.01 \bullet BloodConc_{Peripheral}\\
&r_{Urinereturn} = k_{kidneypermability} \bullet Vasopressin \bullet \left(\left(\frac{Urine_{Mass}}{Urine_{Volume}}\right) - \frac{BloodConc_{Peripheral} \bullet V_{BloodPeripheral}}{V_{PlasmaPeripheral}}\right) \bullet Urine_{Volume}
\end{aligned}
\tag{3}
$$

Where the blood volumes are based on Nadler's Eq. [48], and the plasma volume is estimated using a parameter, $k_{blood\ plasma\ ratio}$, representing the water contents of the blood.

$$
\begin{aligned}
&V_{Blood} = \begin{cases} if male, \frac{2.447 - 0.09516 \bullet age + 0.1074 \bullet height + 0.3362 \bullet weight}{0.84} \bullet 10 \\ if female, \frac{-2.097 + 0.1069 \bullet height + 0.2466 \bullet weight}{0.84} \bullet 10 \end{cases}\\
&V_{BloodCentral} = 0.15 \bullet V_{Blood}\\
&V_{BloodPeripheral} = 0.85 \bullet V_{Blood}\\
&V_{PlasmaPeripheral} = k_{bloodplasmaratio} \bullet V_{BloodPeripheral}
\end{aligned}
\tag{4}
$$

Dynamics of EtG and EtS

EtG and EtS are synthesised from the breakdown of BAC in the liver compartment, diffused into the peripheral blood compartment, and eliminated through the urine.

$$
\begin{aligned}
&\frac{d}{dt}LiverConc = r_{Liver} \bullet \frac{V_{BloodPeripheral}}{V_{Liver}} - rEtOH_{elimination} - r_{EtG} - r_{EtS}\\
&\frac{d}{dt}LiverEtG = r_{EtG} - r_{EtGLiverPeripheral}\\
&\frac{d}{dt}PeripheralEtG = r_{EtGLiverPeripheral} \bullet \frac{V_{Liver}}{V_{BloodPeripheral}} - r_{EtGurine}\\
&\frac{d}{dt}LiverEtS = r_{EtS} - r_{EtSPeripheral}\\
&\frac{d}{dt}PeripheralEtS = r_{EtSPeripheral} \bullet \frac{V_{Liver}}{V_{BloodPeripheral}} - r_{EtSurine}\\
&rEtOH_{elimination} = V_{\max ADH} \bullet \frac{LiverConc}{LiverConc + km_{ADH}} + V_{\max CYP2e1}\\
&\qquad \bullet \frac{LiverConc}{LiverConc + km_{CYP2e1}}\\
&r_{EtG} = V_{\max EtG} \bullet \frac{LiverConc}{LiverConc + km_{EtG}}\\
&r_{EtS} = V_{\max EtS} \bullet \frac{LiverConc}{LiverConc + km_{EtS}}\\
&r_{EtGLiverPeripheral} = LiverEtG - PeripheralEtG\\
&r_{EtSLiverPeripheral} = LiverEtS - PeripheralEtS\\
&r_{EtGurine} = k_{EtGurine} \bullet PeripheralEtG\\
&r_{EtSurine} = k_{EtSurine} \bullet PeripheralEtS
\end{aligned}
\tag{5}
$$

Where the volume of the liver is described according to Vauthey's formula[49].

$$
V_{Liver} = \frac{18.51 \bullet weight + 191.8}{100} \tag{6}
$$

Dynamics of UAC

The urine is handled as a mass and volume, instead of a concentration, as it makes it easier to keep track of consumed liquid that continuously enter the bladder.

$$
\begin{aligned}
&\frac{d}{dt}UrineMassEtOH = +r_{urine} - r_{urinereturn}\\
&\frac{d}{dt}UrineVolume = 0.01 + r_{tissueurine}\\
&\frac{d}{dt}UrineMassEtG = r_{EtGurine} \bullet V_{BloodPeripheral}\\
&\frac{d}{dt}UrineMassEtG = r_{EtSurine} \bullet V_{BloodPeripheral}\\
&r_{tissueurine} = \frac{TissueExtraWater}{Vasopressin} \bullet k_{urinewater}\\
&if urinate \rightarrow \begin{cases} UrineMassEtOH = UrineMassEtOH \bullet \frac{0.05}{UrineVolume} \\ UrineMassEtG = UrineMassEtG \bullet \frac{0.05}{UrineVolume} \\ UrineMassEtS = UrineMassEtS \bullet \frac{0.05}{UrineVolume} \\ UrineVolume = 0.05 \end{cases}
\end{aligned}
\tag{7}
$$

Where 0.05 dL represent the residual volume in the bladder after urination[50].

Dynamics of tissue and vasopressin

$$
\begin{aligned}
&\frac{d}{dt}TissueConc = r_{tissuePeripheral} \bullet \frac{V_{BloodPeripheral}}{V_{Tissue}}\\
&\frac{d}{dt}TissueExtraWater = rvol_{emptying} \bullet 10 - r_{tissueurine}\\
&\frac{d}{dt}Vasopressin = r_{vasopressininflux} - r_{vasopressinclerance}\\
&r_{tissuePeripheral} = BloodConc_{Peripheral} - TissueConc\\
&r_{vasopressininflux} = \frac{k_{basalvasopressin}}{1 + k_{vasopressinBAC} \bullet BloodConc_{Peripheral}}\\
&r_{vasopressinclerance} = Vasopressin \bullet k_{clearancevasopressin}
\end{aligned}
\tag{8}
$$

Where the tissue volume is described as the difference between the TBW, Watson et al.[26], and the other volumes divided into separate compartments in the model.

$$V_{Tissue} = TBW - V_{Blood} - V_{Liver} + TissueExtraWater$$
$$TBW = \begin{cases} if male, \left(0.3669 \bullet height^3 + 0.03219 \bullet weight + 0.6041\right) \bullet 10 \\ if female, \left(0.3561 \bullet height^3 + 0.03308 \bullet weight + 0.1833\right) \bullet 10 \end{cases} \quad (9)$$

Initial values of the model

It was assumed, in the model, that the person has no residual alcohol in the system. Furthermore, it was assumed that the model starts in a fasted state, with no kcal in the system, that the residual volume in the stomach was 0.001 L, and that the residual volume in the bladder was 0.05 dL. The initial value of *Vasopressin* was estimated by assuming mass balance in the first time point. In the case of the Javors experiments[35], the basal values of *PEth* and *PEthBound* were also estimated from the estimated parameter values assuming mass balance in the first time point. Otherwise, they were assumed to be 0. The initial values used are given in Table 1.

Model parameter values

This section gives the optimal parameter values for the connected model when estimated to the estimation dataset (columns θ_{est}*). Furthermore, the bounds used in the optimization for all parameters are also given (columns lower bound and upper bound), see Table 2. $km_{ADH,}km_{CYP2E1}$, and $km_{Gastric}$ were given bounds reported in literature[51].

Model inputs

This section lists the input values the model needs; see Table 3. A detailed overview of all the inputs provided to the model for each dataset is provided in the Supplementary Information, see "3 Input estimations".

Model outputs

This section lists the model outputs, and the scaling performed. $yBrAC_{g201L}$ rescales the plasma concentration of ethanol $BloodConc_{Central}$ into breath concentration using a linear correlation observed between BrAC and BAC measurements by Skaggs et al.[52]. The additional division of 1000 is to go from *g* to *mg*. In Javors et al.[35], the blood concentration was estimated from the breathalyzer test and as such the $yBrAC_{gdL}$ uses $BloodConc_{Central}$ and scales

State	Initial values
$Vol_{Stomach}$	$1.0 \cdot 10^{-3}$
$Kcal_{Liquid}$	0.0
$Kcal_{remain}$	0.0
$MaxKcal_{Solid}$	0.0
$Kcal_{Solid}$	0.0
$EtOH_{Pool}$	0.0
$ConcEtOH_{Stomach}$	0.0
$MassEtOH_{Intestines}$	0.0
BloodConcCentral	0.0
BloodConcPeripheral	0.0
TissueConc	0.0
LiverConc	0.0
LiverEtG	0.0
PeripheralEtG	0.0
LiverEtS	0.0
PeripheralEtS	0.0
$Plasma_{Acetate}$	0.0
TissueExtraWater	0.0
Vasopressin	*estimated*
UrineMassEtOH	0.0
UrineVolume	0.05
UrineMassEtG	0.0
UrineMassEtS	0.0
PEth	*estimated*
$PEth_{Bound}$	*estimated*
timeElapsed	0.0

Table 1. Initial values of the model.

Parameter	θ_{est}*	lower bound	upper bound
VmaxGastric	0.10028847533601028	$1{\cdot}10^{-5}$	$1{\cdot}10^{5}$
KmGastric	0.8115471295053232	$2.766{\cdot}10^{1}$	$1.844{\cdot}10^{3}$
k_kcalscaling	0.026009077044725923	$1{\cdot}10^{-5}$	$1{\cdot}10^{5}$
km_kcal	7219.025648168511	$1{\cdot}10^{-5}$	$1{\cdot}10^{5}$
n_kcal	2.9350431505014307	$1{\cdot}10^{-1}$	$4{\cdot}10^{0}$
k_poolIn	0.049215056963481905	$1{\cdot}10^{-5}$	$1{\cdot}10^{5}$
k_poolOut	0.00011026963373147828	$1{\cdot}10^{-7}$	$1{\cdot}10^{5}$
VmaxADHSto	383.0316652068957	$1{\cdot}10^{-5}$	$1{\cdot}10^{5}$
KmADHSto	1750.8565753331234	$2.766{\cdot}10^{2}$	$1.844{\cdot}10^{3}$
k_EtOHuptake	0.05085931578651339	$1{\cdot}10^{-5}$	$1{\cdot}10^{5}$
k_equalize	3.364285096106452	$1{\cdot}10^{-5}$	$1{\cdot}10^{5}$
k_equalize_liver	0.5664934932515018	$1{\cdot}10^{-5}$	$1{\cdot}10^{5}$
VmaxADH1	7.490115599723829	$1{\cdot}10^{-5}$	$1{\cdot}10^{5}$
VmaxCYP2E1	0.7715882956131286	$1{\cdot}10^{-5}$	$1{\cdot}10^{5}$
KmADH1	2.13180346563429	$9.22{\cdot}10^{-1}$	$9.22{\cdot}10^{0}$
KmCYP2E1	45.98540429542478	$3.688{\cdot}10^{1}$	$4.61{\cdot}10^{1}$
k_food_clearance	0.1350242774593947	$1{\cdot}10^{-5}$	$1{\cdot}10^{5}$
k_acetate	1.1650870599405063	$1{\cdot}10^{-5}$	$1{\cdot}10^{5}$
k_blood_plasma_ratio	0.6871729866586396	$1{\cdot}10^{-1}$	$1{\cdot}10^{0}$
k_urine_water	5.961711956546037	$1{\cdot}10^{-5}$	$1{\cdot}10^{5}$
k_basal_vasopressin	0.3849587409310818	$1{\cdot}10^{-5}$	$1{\cdot}10^{5}$
k_vasopressin_BAC	74740.43401768291	$1{\cdot}10^{-5}$	$1{\cdot}10^{5}$
k_clearance_vasopressin	0.0006626630440471179	$1{\cdot}10^{-5}$	$1{\cdot}10^{5}$
k_kidney_permability	2.5215624280668018e-05	$1{\cdot}10^{-5}$	$1{\cdot}10^{5}$
VmaxEtG	0.6461457040480787	$1{\cdot}10^{-5}$	$1{\cdot}10^{5}$
KmEtG	29854.322456892394	$1{\cdot}10^{-5}$	$1{\cdot}10^{5}$
VmaxEtS	0.011876595138349037	$1{\cdot}10^{-5}$	$1{\cdot}10^{5}$
KmEtS	414.40740948670106	$1{\cdot}10^{-5}$	$1{\cdot}10^{5}$
k_EtG_urine	0.0024879684263205454	$1{\cdot}10^{-5}$	$1{\cdot}10^{5}$
k_EtS_urine	0.014152433882270748	$1{\cdot}10^{-5}$	$1{\cdot}10^{5}$
k_PEth	0.13959486810293995	$1{\cdot}10^{-7}$	$1{\cdot}10^{3}$
k_PEth_clearance	0.001460712263112933	$1{\cdot}10^{-7}$	$1{\cdot}10^{3}$
k_PEth_bind	0.07805739912357477	$1{\cdot}10^{-7}$	$1{\cdot}10^{3}$
k_PEth_release	0.002851044320061577	$1{\cdot}10^{-7}$	$1{\cdot}10^{3}$

Table 2. Parameter values and parameter estimation bounds.

Input variable	Description
EtOHConc	Ethanol concentration
volDrinkPerTime	Consumed volume per minute
kcalLiquidPerVol	Amount of kcal per liter beverage
MealKcal	Amount of kcal in a meal
sex	Male (1) or Female (0)
weight	Weight in kg
height	Height in meter
age	The age in years
urinate	Time of urination

Table 3. Input information to the model.

it with 1000 to get g/dL. *yAcetate* is divided by 10.2 to convert the concentration unit *mg/dL* to *mM*. *yUAC* is calculated from the mass of EtOH in the urine and the volume of urine in the bladder.

$$\begin{aligned}
yGastricVolume &= Vol_{Stomach} \\
yEtOH &= BloodConc_{Peripheral} \\
yBrAC_{g210L} &= 0.840 * \left(\frac{BloodConc_{Central}}{1000}\right) + 0.00367 \\
yBrAC_{gdL} &= \frac{BloodConc_{Central}}{1000} \\
yAcetate &= Plasma_{Acetate} \cdot \frac{1}{10.2} \\
yPEth &= PEth \\
yUAC &= \frac{UrineMassEtOH}{Urine_{Volume}} \\
yEtG &= Peripheral_{EtG} \\
yEtS &= Peripheral_{EtS}
\end{aligned} \tag{10}$$

Parameter estimation

All model analysis was performed using Python 3.10.4 and plotting using Python 3.12.3[53]. The simulations were carried out using the SUND toolbox[54]. For model parameter estimation the dual annealing[55] and differential evolution[56,57] algorithms, provided by SciPy[58], were used.

Parameter estimation was done by quantifying the model performance, using the model output ? to calculate the traditional weighted least squares cost function defined as

$$V(\theta) = \sum_i \sum_k \sum_j \left(\frac{y_{i,k,j}(t_{i,k,j}) - \hat{y}_{i,k,j}(t_{i,k,j},\theta)}{SEM_{i,k,j}(t_{i,k,j})}\right)^2 \tag{11}$$

$$SEM_{i,k,j} = \frac{\sigma_{i,k,j}(t_{i,k,j})}{\sqrt{n_{i,k,j}(t_{i,k,j})}} \tag{12}$$

where, θ is the model parameters; $y_{i,k,j}(t_{i,k,j})$ is the measured data from a study *i*, and from on type of measure *k*, at time point *j*; $?_{i,k,j}(t_{i,k,j},\theta)$ is the simulation value for a given experiment setup *i*, type of measure *k*, and time point *j*. SEM is the standard error of the mean, which is the sample standard deviation, $\sigma_{i,k,j}(t_{i,k,j})$ divided with the square root of the number of repeats, $n_{i,k,j}(t_{i,k,j})$ at each time point. The value of the cost function, $V(\theta)$, is then minimized by tuning the values of the parameters, typically referred to as parameter estimation.

To evaluate the new model, a χ^2-test for the size of the residuals, with the null hypothesis that the experimental data have been generated by the model, and that the experimental noise is additive and normally distributed was performed. In practice, the cost function value was compared to a χ^2 test statistic,$T^o_{\chi 2}$. The test statistic χ^2 cumulative density function,

$$T^o_{\chi 2} = \mathcal{F}^{\mathrm{cdf-inv}}_{\chi 2}(1-\alpha, v) \tag{13}$$

where $\mathcal{F}^{\mathrm{cdf-inv}}_{\chi 2}$ is the inverse density function; and α is the significance level (α = 0.05, was used) and *v* is the degrees of freedom, which was equal to the number of data points in the estimation dataset (674 in total, all timepoints over all experiments). In practice, the model is rejected if the model cost is larger than the χ^2 -threshold ($T^o_{\chi 2}$).

Uncertainty estimation

The model simulation uncertainty was gathered as proposed in[59] and is visualized as the uncertainty areas in the figures. The model uncertainty is estimated by dividing the problem into multiple optimization problems, with one problem per model property ($\widehat{p}$). In this work, the property $\widehat{p}$ corresponds to either a simulation at a specific time point *j*, $\widehat{y}(t_j,\theta)$, or a parameter value $\widehat{\theta}_m$. Each problem is solved by maximizing and minimizing the property value, while satisfying that the cost ($V(\theta)$) is below the χ^2-threshold ($T^o_{\chi 2}$). By identifying the maximal and minimal value of the model property ($\widehat{p}_{max}$ and $\widehat{p}_{min}$), the boundary values of the property uncertainty area are found. Mathematically, this operation for the parameter values is formulated as,

$$minimize \widehat{\theta}_m \tag{14a}$$

$$subject to V(\theta) < T^o_{\chi 2} \tag{14b}$$

where $\widehat{\theta}_m$ is minimized to find the lower value of the parameter, while also satisfying that the cost ($V(\theta)$) is below the χ^2-threshold ($T^o_{\chi 2}$). To find the upper bound of the uncertainty area the problem is maximized instead. In practice, the constraint (Eq. 4b) can be relaxed into the objective function as a L1 penalty term with an offset if $V(\theta) > T^o_{\chi 2}$.

$$minimize\, \widehat{\theta}_m + penalty \tag{15a}$$

$$where\, penalty = \begin{cases} \left|\widehat{\theta}_m\right| + \left|\widehat{\theta}_{m,0}\right| * \left(1 + \left(V(\theta) - T^o_{\chi 2}\right)\right), if\, V(\theta) > T^o_{\chi 2} \\ 0,\, otherwise \end{cases} \tag{15b}$$

Here, the penalty is scaled with the initial value of the parameter, $\widehat{\theta}_{m,0}$ and the offset between the cost and the χ^2-threshold ($V(\theta) - T^o_{\chi 2}$). To maximize the parameter$\widehat{\theta}$, and thus finding the upper bound of the uncertainty area, the problem is solved as a minimization problem. This is done by substituting $\widehat{\theta}_m$ with $-\widehat{\theta}_m$ in the objective function. To solve the problem for the model simulation at a specific time point, $\widehat{y}(t_j, \theta)$, the problem is formulated as follows,

$$minimize\, \widehat{y}(t_j, \theta) + penalty \tag{16a}$$

$$where\, penalty = \begin{cases} \left|\widehat{y}(t_j, \theta)\right| + \left|\widehat{y}(t_j, \theta)_0\right| * \left(1 + \left(V(\theta) - T^o_{\chi 2}\right)\right), if\, V(\theta) > T^o_{\chi 2} \\ 0,\, otherwise \end{cases} \tag{16b}$$

Here, the penalty is scaled with the initial value of the parameter, $\widehat{y}(t_j, \theta)_0$, and the offset between the cost and the χ^2-threshold ($V(\theta) - T^o_{\chi 2}$). To maximize the model simulation at time point *j*, ($\widehat{y}(t_j, \theta)$, and thus finding the upper bound of the uncertainty area, the problem is solved as a minimization problem. This is done by substituting $\widehat{y}(t_j, \theta)$ with $-\widehat{y}(t_j, \theta)$ in the objective function.

The experimental data used for the modelling

This work incorporates a wide variety of data for the model estimation and validation - details of these data are given below.

The gastric emptying module was evaluated with three studies from Okabe et al.; the first explored the effect of caloric content[32], the second the influence of caloric density[33], and the third the effect of alcoholic calories[9].

A variety of studies observing the BAC levels were included. The effect of a meal was studied in Jones et al.[29]. Mitchell et al. investigated the effect of different alcoholic compositions[34]. Sarkola et al. studied the BAC and acetate response following one drink[36]. Frezza et al. compared the effect between females and males[37]. Javors et al. investigated the BrAC and PEth levels after a drink[35]. Kronstrand et al.[12]. and Hoiseth et al.[11] investigate the BAC response to double dosing of different alcohol types and volumes.

The alcohol marker UAC was collected by Kronstrand et al.[12]. and Hoiseth et al.[11]. EtG and EtS markers were reported by Hoiseth et al.[11].

Wang et al. presented the data used for the validation analysis, which consisted of BAC, EtG, and EtS measurements[38].

We collected new data from two individuals during a sequential drink intervention study performed by the National Board of Forensic Medicine. All methods were performed in accordance with relevant guidelines and regulations. Written informed consent was obtained from all participants, and the study was approved by the Swedish Ethical Review Authority (2023-02640-01).

Data availability

All data used for model estimation and validation can be accessed from the original publications. The new data is available from the Supplementary Information. We provide all model related data files and parameter values in our public code repository (https://github.com/Podde1/alcohol-secondary-metabolites/), with a permanent copy available at Zenodo (DOI: https://doi.org/10.5281/zenodo.17609970).

Code availability

All related scripts and data files are provided in our GitHub repository (https://github.com/Podde1/alcohol-secondary-metabolites/), with a permanent copy available at Zenodo (DOI: https://doi.org/10.5281/zenodo.17609970). Additionally, a user interface for the model implemented as a web application is provided. This application is available at (https://alcohol.streamlit.app/), with the source code available from our GitHub repository (https://github.com/willov/alcohol_app/) - with a permanent copy available at Zenodo (DOI: https://doi.org/10.5281/zenodo.17609892).

Received: 22 January 2026; Accepted: 9 March 2026
Published online: 18 March 2026

References

1. Jones, A. W. Measuring Alcohol in Blood and Breath for Forensic Purposes - A Historical Review. *Forensic Sci. Rev.* **8** (1), 13–44 (1996). PubMed PMID: 26270605.
2. Kim, S. H., Son, H. W., Lee, T. M. & Baek, H. J. Drunk Driver Detection Using Multiple Non-Invasive Biosignals. *Sensors* **25** (5), 1281 (2025). doi:10.3390/s25051281 PubMed PMID: 40096026; PubMed Central PMCID: PMC11902798.
3. Aston, E. R. & Liguori, A. Self-estimation of blood alcohol concentration: A review. *Addict. Behav.* **38** (4), 1944–1951. https://doi.org/10.1016/j.addbeh.2012.12.017 (2013).
4. Jones, A. W. Alcohol, its absorption, distribution, metabolism, and excretion in the body and pharmacokinetic calculations. *WIREs Forensic Sci.* **1** (5), e1340. https://doi.org/10.1002/wfs2.1340 (2019).
5. Jones, A. W. Pharmacokinetics of Ethanol — Issues of Forensic Importance. *Forensic Sci. Rev.* **23** (2), 91–136 (2011).

6. Maskell, P. D., Jones, A. W., Savage, A. & Scott-Ham, M. Evidence based survey of the distribution volume of ethanol: Comparison of empirically determined values with anthropometric measures. *Forensic Sci. Int.* **294**, 124–131. https://doi.org/10.1016/j.forsciint.2018.10.033 (2019).
7. Jones, A. W. Evidence-based survey of the elimination rates of ethanol from blood with applications in forensic casework. *Forensic Sci. Int.* **200** (1), 1–20. https://doi.org/10.1016/j.forsciint.2010.02.021 (2010).
8. Kechagias, Jönsson, J. Impact of gastric emptying on the pharmacokinetics of ethanol as influenced by cisapride. *Br. J. Clin. Pharmacol.* **48** (5), 728–732. https://doi.org/10.1046/j.1365-2125.1999.00080.x (1999).
9. Okabe, T., Terashima, H. & Sakamoto, A. Comparison of Gastric Emptying Time after the Ingestion of Whisky with Isocalorically Adjusted Glucose Solution. *J. Nutr. Metab.* **2022**, 6137230. https://doi.org/10.1155/2022/6137230 (2022). PubMed PMID: 35734752; PubMed Central PMCID: PMC9209003.
10. Franke, A., Teyssen, S., Harder, H. & Singer, M. V. Effect of ethanol and some alcoholic beverages on gastric emptying in humans. *Scand. J. Gastroenterol.* **39** (7), 638–644 (2004). doi:10.1080/00365520410005009 PubMed PMID: 15370684.
11. Höiseth, G. et al. Evaluating the hip-flask defence using analytical data from ethanol and ethyl glucuronide. A comparison of two models. *Forensic Sci. Int.* **316**, 110409. https://doi.org/10.1016/j.forsciint.2020.110409 (2020).
12. Kronstrand, C. et al. Evaluating the hip-flask defence in subjects with alcohol on board: An experimental study. *Forensic Sci. Int.* **294**, 189–195. https://doi.org/10.1016/j.forsciint.2018.11.014 (2019).
13. Iffland, R. & Jones, A. W. Evaluating Alleged Drinking after Driving - The Hip-Flask Defence: Part 1. Double Blood Samples and Urine-to-Blood Alcohol Relationship. *Med. Sci. Law.* **42** (3), 207–224 (2002).
14. Palmer, R. B. A review of the use of ethyl glucuronide as a marker for ethanol consumption in forensic and clinical medicine. *Semin Diagn. Pathol.* **26** (1), 18–27. https://doi.org/10.1053/j.semdp.2008.12.005 (2009). Toxicologic/Environmental Pathology.
15. Widmark, E. M. P. *Principles and applications of medicolegal alcohol determination. Davis, Calif* 163 (Biomedical, 1981).
16. Zekan, P. et al. Pharmacokinetic Analysis of Ethanol in a Human Study: New Modification of Mathematic Model. *Toxics* **11** (9), 793. https://doi.org/10.3390/toxics11090793 (2023). PubMed PMID: 37755803; PubMed Central PMCID: PMC10534806.
17. Sadighi, A., Leggio, L. & Akhlaghi, F. Development of a Physiologically Based Pharmacokinetic Model for Prediction of Ethanol Concentration-Time Profile in Different Organs. *Alcohol Alcohol.* **56** (4), 401–414. https://doi.org/10.1093/alcalc/agaa129 (2021).
18. Zhang, Y., Wu, C. & Wan, J. Development and validation of a model to predict blood alcohol concentrations: Updating the NHTSA equation. *Addict. Behav.* **71**, 46–53. https://doi.org/10.1016/j.addbeh.2017.02.022 (2017).
19. Moore, S. et al. Pairing food and drink: A physiological model of blood ethanol levels for a variety of drinking behaviors. *Math. Biosci.* **345**, 108778. https://doi.org/10.1016/j.mbs.2022.108778 (2022).
20. Droenner, P., Schmitt, G., Aderjan, R. & Zimmer, H. A kinetic model describing the pharmacokinetics of ethyl glucuronide in humans. *Forensic Sci. Int.* **126** (1), 24–29. https://doi.org/10.1016/S0379-0738(02)00025-7 (2002).
21. Schmitt, G., Halter, C. C., Aderjan, R., Auwaerter, V. & Weinmann, W. Computer assisted modeling of ethyl sulfate pharmacokinetics. *Forensic Sci. Int.* **194** (1), 34–38. https://doi.org/10.1016/j.forsciint.2009.10.004 (2010).
22. Smith, G. I., Commean, P. K., Reeds, D. N., Klein, S. & Mittendorfer, B. Effect of protein supplementation during diet-induced weight loss on muscle mass and strength: a randomized controlled study. *Obes. Silver Spring Md.* **26** (5), 854–861. https://doi.org/10.1002/oby.22169 (2018). PubMed PMID: 29687650; PubMed Central PMCID: PMC5918424.
23. Herrgårdh, T. et al. A multi-scale digital twin for adiposity-driven insulin resistance in humans: diet and drug effects. *Diabetol. Metab. Syndr.* **15**, 250. https://doi.org/10.1186/s13098-023-01223-6 (2023). PubMed PMID: 38044443; PubMed Central PMCID: PMC10694923.
24. Erdős, B. et al. Leveraging continuous glucose monitoring for personalized modeling of insulin-regulated glucose metabolism. *Sci. Rep.* **14** (1), 8037. https://doi.org/10.1038/s41598-024-58703-6 (2024).
25. Podéus, H. et al. A physiologically-based digital twin for alcohol consumption—predicting real-life drinking responses and long-term plasma PEth. *Npj Digit. Med.* **7** (1), 1–18. https://doi.org/10.1038/s41746-024-01089-6 (2024).
26. Watson, P. E., Watson, I. D. & Batt, R. D. Prediction of blood alcohol concentrations in human subjects. Updating the Widmark Equation. *J. Stud. Alcohol.* **42** (7), 547–556. https://doi.org/10.15288/jsa.1981.42.547 (1981).
27. Polhuis, K. C. M. M., Wijnen, A. H. C., Sierksma, A., Calame, W. & Tieland, M. The Diuretic Action of Weak and Strong Alcoholic Beverages in Elderly Men: A Randomized Diet-Controlled Crossover Trial. *Nutrients* **9** (7), 660. https://doi.org/10.3390/nu9070660 (2017). PubMed PMID: 28657601; PubMed Central PMCID: PMC5537780.
28. Eisenhofer, G. & Johnson, R. H. Effect of ethanol ingestion on plasma vasopressin and water balance in humans. *Am. J. Physiol-Regul Integr. Comp. Physiol.* **242** (5), R522–R527. https://doi.org/10.1152/ajpregu.1982.242.5.R522 (1982).
29. Jones, A. W., Jönsson, K. Å. & Kechagias, S. Effect of high-fat, high-protein, and high-carbohydrate meals on the pharmacokinetics of a small dose of ethanol. *Br. J. Clin. Pharmacol.* **44** (6), 521–526. https://doi.org/10.1046/j.1365-2125.1997.t01-1-00620.x (1997).
30. Hahn, R. G. et al. *Alcohol Alcohol* ;**29**(6):673–699. doi:https://doi.org/10.1093/oxfordjournals.alcalc.a045602 (1994).
31. Ramchandani, V. A., Kwo, P. Y. & Li, T. K. Effect of Food and Food Composition on Alcohol Elimination Rates in Healthy Men and Women. *J. Clin. Pharmacol.* **41** (12), 1345–1350. https://doi.org/10.1177/00912700122012814 (2001).
32. Okabe, T., Terashima, H. & Sakamoto, A. Determinants of liquid gastric emptying: comparisons between milk and isocalorically adjusted clear fluids. *Br. J. Anaesth.* **114** (1), 77–82. https://doi.org/10.1093/bja/aeu338 (2015).
33. Okabe, T., Terashima, H. & Sakamoto, A. What is the manner of gastric emptying after ingestion of liquids with differences in the volume under uniform glucose-based energy content? *Clin. Nutr.* **36** (5), 1283–1287. https://doi.org/10.1016/j.clnu.2016.08.014 (2017).
34. Mitchell, M. C. Jr, Teigen, E. L. & Ramchandani, V. A. Absorption and Peak Blood Alcohol Concentration After Drinking Beer, Wine, or Spirits. *Alcohol Clin. Exp. Res.* **38** (5), 1200–1204. https://doi.org/10.1111/acer.12355 (2014).
35. Javors, M. A., Hill-Kapturczak, N., Roache, J. D., Karns-Wright, T. E. & Dougherty, D. M. Characterization of the Pharmacokinetics of Phosphatidylethanol 16:0/18:1 and 16:0/18:2 in Human Whole Blood After Alcohol Consumption in a Clinical Laboratory Study. *Alcohol Clin. Exp. Res.* **40** (6), 1228–1234. https://doi.org/10.1111/acer.13062 (2016).
36. Sarkola, T., Iles, M. R., Kohlenberg-Mueller, K., Eriksson, C. J. P. & Ethanol Acetaldehyde, Acetate, and Lactate Levels After Alcohol Intake in White Men and Women: Effect of 4-Methylpyrazole. *Alcohol Clin. Exp. Res.* **26** (2), 239–245. https://doi.org/10.1111/j.1530-0277.2002.tb02530.x (2002).
37. Frezza, M. et al. High Blood Alcohol Levels in Women. *N Engl. J. Med.* **322** (2), 95–99. 10.1056 (1990). /NEJM199001113220205 PubMed PMID: 2248624.
38. Wang, L. et al. Estimating the time of last drinking from blood ethyl glucuronide and ethyl sulphate concentrations. *Sci. Rep.* **12** (1), 1. https://doi.org/10.1038/s41598-022-18527-8 (2022).
39. Stachel, N. & Skopp, G. Identification and characterization of sulfonyltransferases catalyzing ethyl sulfate formation and their inhibition by polyphenols. *Int. J. Legal Med.* **130** (1), 139–146. https://doi.org/10.1007/s00414-015-1159-5 (2016).
40. Schwab, N. & Skopp, G. Identification and preliminary characterization of UDP-glucuronosyltransferases catalyzing formation of ethyl glucuronide. *Anal. Bioanal Chem.* **406** (9), 2325–2332. https://doi.org/10.1007/s00216-014-7675-1 (2014).
41. Stachel, N. & Skopp, G. In vitro formation of ethyl glucuronide and ethyl sulfate. *Toxichem Krimtech.* **82**, 239–245 (2015).
42. Foti, R. S. & Fisher, M. B. Assessment of UDP-glucuronosyltransferase catalyzed formation of ethyl glucuronide in human liver microsomes and recombinant UGTs. *Forensic Sci. Int.* **153** (2), 109–116. https://doi.org/10.1016/j.forsciint.2004.12.003 (2005).
43. Stachel, N. & Skopp, G. Formation and inhibition of ethyl glucuronide and ethyl sulfate. *Forensic Sci. Int.* **Special Issue on the 53rd Annual Meeting of the International Association of Forensic Toxicologists (TIAFT)265**, 61–64. https://doi.org/10.1016/j.forsciint.2016.01.009 (2016).

44. Edenberg, H. J. The Genetics of Alcohol Metabolism: Role of Alcohol Dehydrogenase and Aldehyde Dehydrogenase Variants. *Alcohol Res. Health.* **30** (1), 5–13 (2007). PubMed PMID: 17718394; PubMed Central PMCID: PMC3860432.
45. Rajendram, R., Hunter, R., Preedy, V. & Peters, T. ALCOHOL | Absorption, Metabolism and Physiological Effects. In: Caballero B, editor. Encyclopedia of Human Nutrition (Second Edition) [Internet]. Oxford: Elsevier; [cited 2022 Nov 15]. pp. 48–57. Available from: https://doi.org/10.1016/B0-12-226694-3/00006-X (2005).
46. Oneta, C. M. et al. Dynamics of cytochrome P4502E1 activity in man: induction by ethanol and disappearance during withdrawal phase. *J. Hepatol.* **36** (1), 47–52. https://doi.org/10.1016/S0168-8278(01)00223-9 (2002).
47. Liangpunsakul, S. et al. Activity of CYP2E1 and CYP3A enzymes in adults with moderate alcohol consumption: A comparison with nonalcoholics. *Hepatology* **41** (5), 1144–1150. https://doi.org/10.1002/hep.20673 (2005).
48. Nadler, S. B., Hidalgo, J. H. & Bloch, T. Prediction of blood volume in normal human adults. *Surgery* **51** (2), 224–232 (1962). PubMed PMID: 21936146.
49. Vauthey, J. N. et al. Body surface area and body weight predict total liver volume in Western adults. *Liver Transpl.* **8** (3), 233–240. https://doi.org/10.1053/jlts.2002.31654 (2002).
50. Ballstaedt, L., Leslie, S. W. & Woodbury, B. Bladder Post Void Residual Volume. In: StatPearls [Internet]. Treasure Island (FL): StatPearls Publishing; 2024 [cited 2024 Dec 12]. Available from: http://www.ncbi.nlm.nih.gov/books/NBK539839/ PubMed PMID: 30969661.
51. Lieber, C. & 2 - Alcohol Metabolism. : General Aspects Original studies were supported, in part, by NIH grants AA11115, the Department of Veterans Affairs, the Kingsbridge Research and the Christopher D. Smithers Foundations. The author is grateful to Ms Y. Rodriguez for the skillful typing of this document. In: Preedy VR, Watson RR, editors. Comprehensive Handbook of Alcohol Related Pathology [Internet]. Oxford: Academic Press; [cited 2023 May 26]. pp. 15–26. Available from: https://www.sciencedirect.com/science/article/pii/B9780125643702500040 (2005). https://doi.org/10.1016/B978-012564370-2/50004-0
52. Skaggs, L., Heizler, A., Kalscheur, D., Miles, A. & Barkholtz, H. M. Comparison of Breath- and Blood-Alcohol Concentrations in a Controlled Drinking Study. *J. Anal. Toxicol.* **46** (6), 683–688. https://doi.org/10.1093/jat/bkab086 (2022).
53. Van Rossum, G. & Drake, F. L. *Python 3 Reference Manual* (CreateSpace, 2009).
54. Podéus, H. et al. SUND: simulation using nonlinear dynamic models - a toolbox for simulating multi-level, time-dynamic systems in a modular way [Internet]. arXiv; [cited 2025 Oct 19]. Available from: http://arxiv.org/abs/2510.13932 (2025). https://doi.org/10.48550/arXiv.2510.13932
55. Xiang, Y., Sun, D. Y., Fan, W. & Gong, X. G. Generalized simulated annealing algorithm and its application to the Thomson model. *Phys. Lett. A.* **233** (3), 216–220. https://doi.org/10.1016/S0375-9601(97)00474-X (1997).
56. Qiang, J. & Mitchell, C. A Unified Differential Evolution Algorithm for Global Optimization.
57. Wormington, M., Panaccione, C., Matney, K. M. & Bowen, D. K. Characterization of structures from X-ray scattering data using genetic algorithms. Bowen DK, Tanner BK, editors. Philos Trans R Soc Lond Ser Math Phys Eng Sci. 357(1761), 2827–48. https://doi.org/10.1098/rsta.1999.0469 (1999).
58. Virtanen, P. et al. SciPy 1.0: fundamental algorithms for scientific computing in Python. *Nat. Methods.* **17** (3), 261–272. https://doi.org/10.1038/s41592-019-0686-2 (2020).
59. Cedersund, G. Conclusions via unique predictions obtained despite unidentifiability – new definitions and a general method. *FEBS J.* **279** (18), 3513–3527. https://doi.org/10.1111/j.1742-4658.2012.08725.x (2012).

Acknowledgements

The computations were enabled by resources provided by the National Supercomputer Centre (NSC), funded by Linköping University.

Author contributions

**Conceptualization: ** HP, GJ, CS, EN, RK, and WL. **Formal model analysis: ** HP, CS, and WL. **Data curation: ** HP, GJ, CS, RK, and WL. **Visualization: ** HP, CS, and WL. **Supervision: ** GC, EN, RK, GJ, and WL. **Funding acquisition: ** GJ, GC, EN, and WL.All authors were involved in writing and reviewing the manuscript. All authors read and approved the final manuscript.

Funding

Open access funding provided by Linköping University. The authors acknowledge financial support from: GC acknowledges support from the Swedish Research Council (2023–03186, 2023–05460), VINNOVA (VisualSweden), the Horizon Europe project STRATIF-AI (101080875), and ALF (RÖ-1001928). GC and WL acknowledge support from the Exploring Inflammation in Health and Disease (X-HiDE) Consortium - a strategic research profile at Örebro University funded by the Knowledge Foundation (20200017). EN acknowledges support from the Swedish Research council (2019–03767), and the Swedish Fund for Research without Animal Experiments (S2021-0008, F2022-02). WL acknowledges support from the Area of Strength e-Health at Linköping University and Region Östergötland. WL and GE acknowledge support from the Strategic Research Area in Forensic Sciences. GJ and RK acknowledges support from the strategic research area in Forensic Science at Linköping University (SoFo 2022-09) funded by the National Board of Forensic Medicine and Linköping University. The funders had no role in study design, data collection and analysis, decision to publish, or preparation of the manuscript.

Declarations

Competing interests

The authors declare no competing interests.

Additional information

Supplementary Information The online version contains supplementary material available at https://doi.org/10.1038/s41598-026-44093-4.

Correspondence and requests for materials should be addressed to G.C.